

## Supporting Information

### Nitrogen-doped graphene encapsulated cobalt iron sulfide as an advanced electrode for high-performance asymmetric supercapacitors

Yazan Al Haj,<sup>a</sup> Jayaraman Balamurugan,<sup>a</sup> Nam Hoon Kim,<sup>a,\*</sup> Joong Hee Lee<sup>a,b\*</sup>

<sup>a</sup>Advanced Materials Institute of BIN Convergence Technology (BK21 Plus Global) & Department of BIN Convergence Technology, Chonbuk National University, Jeonju, Jeonbuk, 54896, Republic of Korea

<sup>b</sup>Carbon Composite Research Centre, Department of Polymer - Nano Science and Technology, Chonbuk National University, Jeonju, Jeonbuk, 54896, Republic of Korea

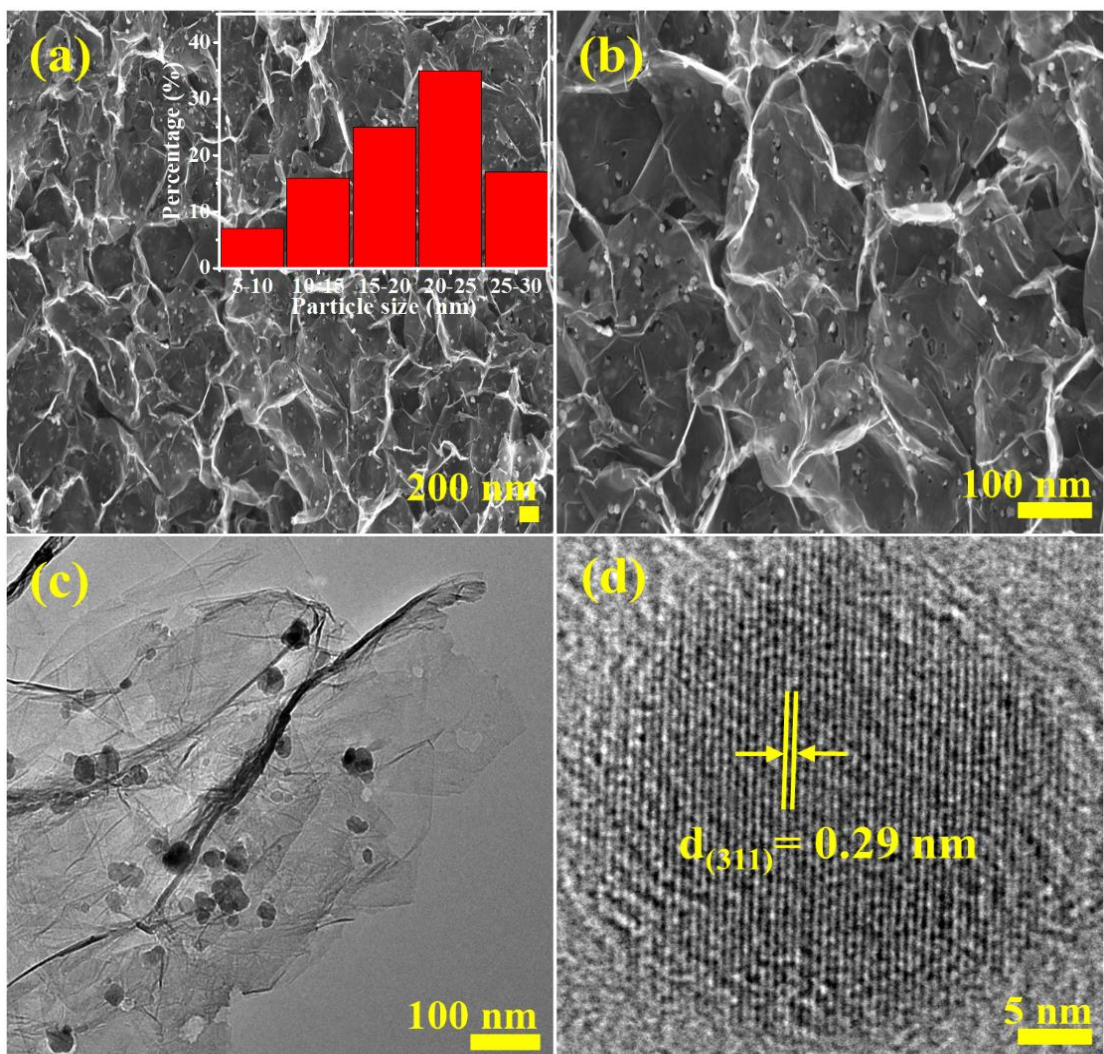


**Fig. S1** (a and b) FE-SEM images with different magnifications (inset shows the particle size distribution), (c) TEM image, and (d) HR-TEM image of  $\text{Co}_8\text{FeS}_8/\text{NG}$ .

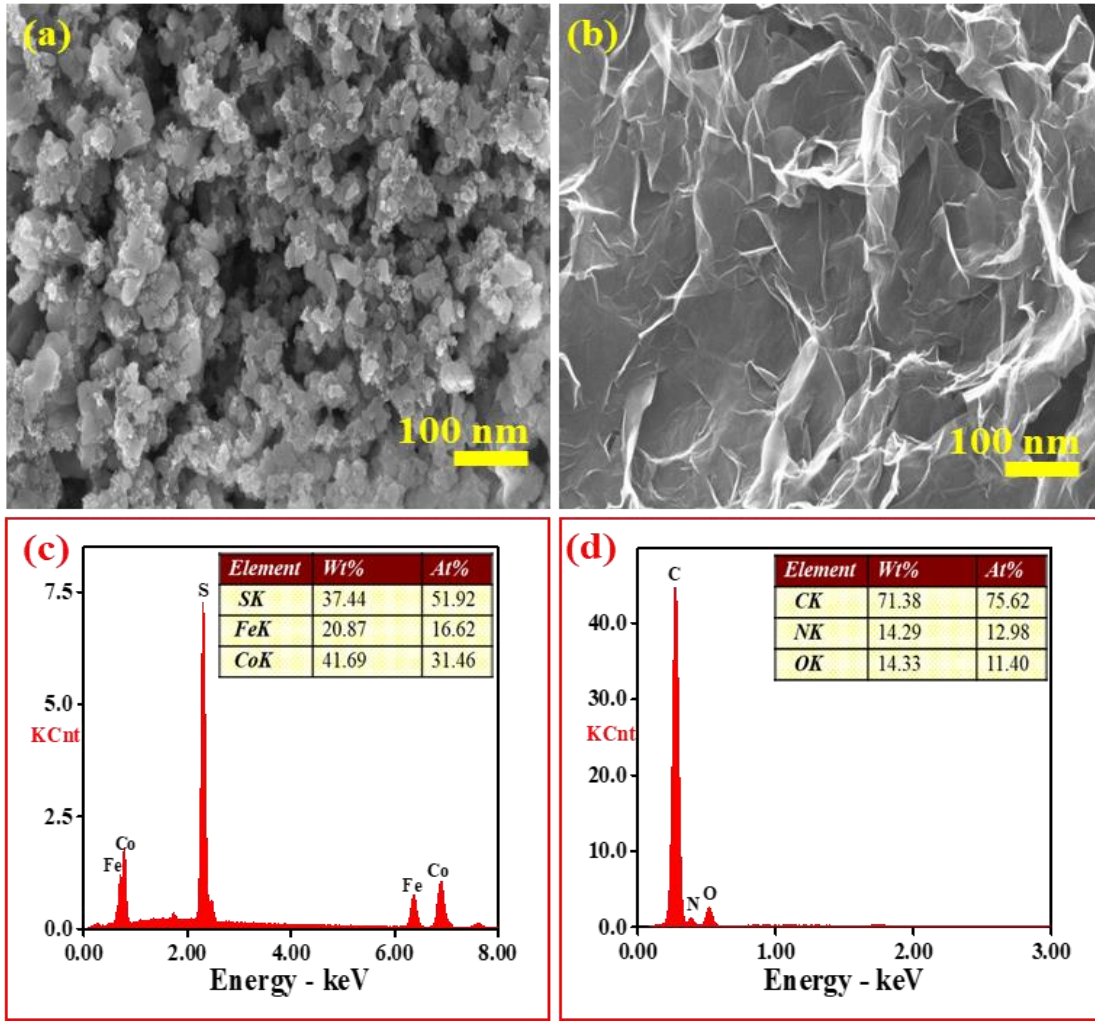


**Fig. S2** (a and b) FE-SEM images, and (c and d) EDAX spectra of pristine Co<sub>8</sub>FeS<sub>8</sub> and pristine NG, respectively.

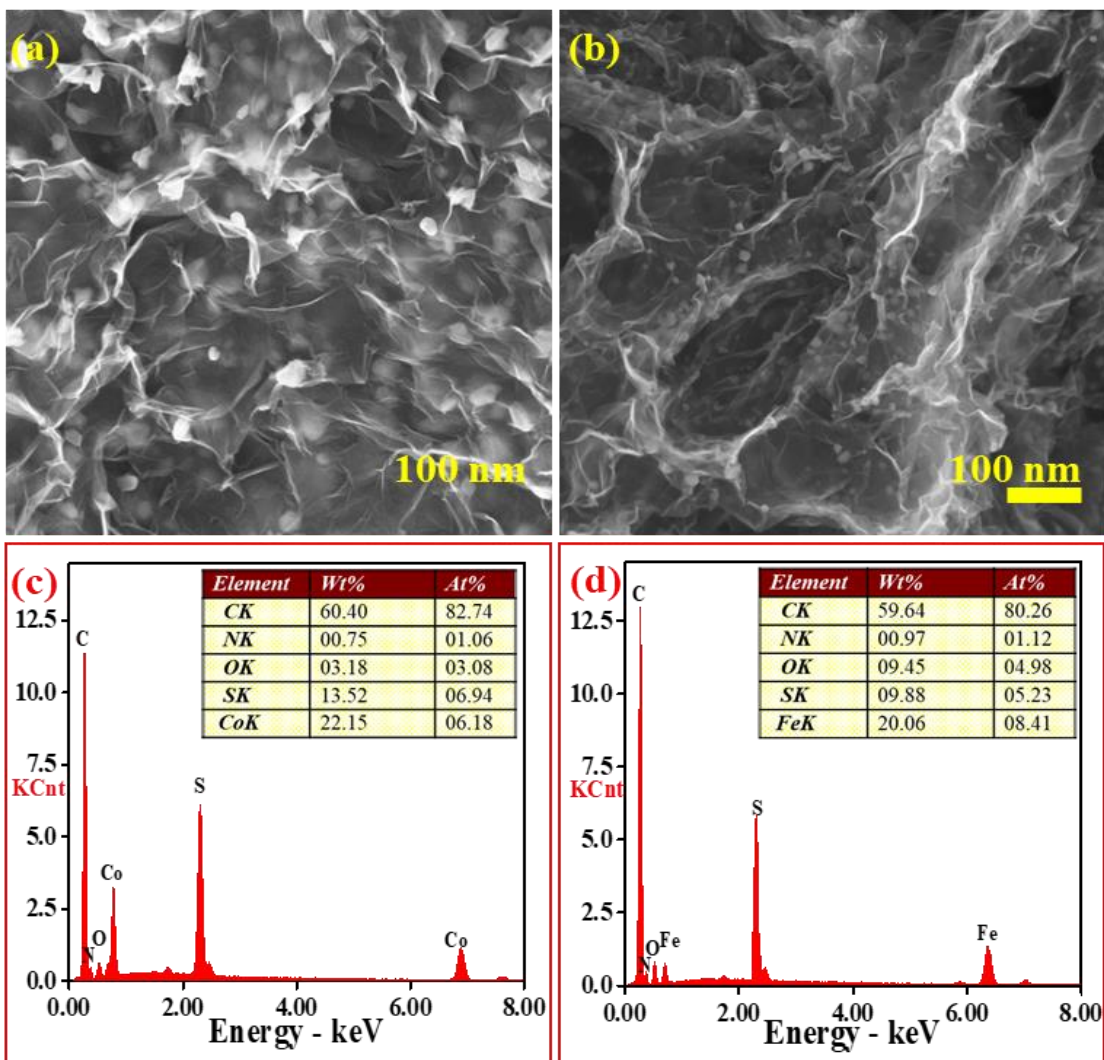


**Fig. S3** (a and b) FE-SEM images, and (c and d) EDAX spectra of pristine  $\text{Co}_9\text{S}_8$ @NG and FeS@NG, respectively.

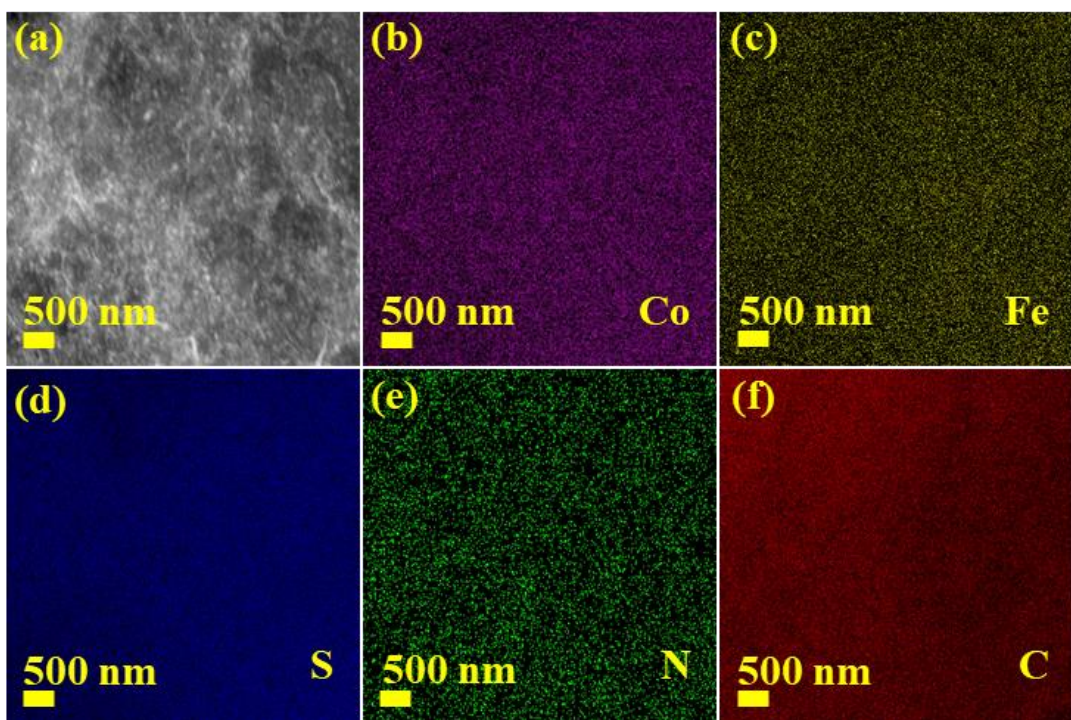


**Fig. S4** SEM-EDS color mapping of cobalt, iron, sulfur, nitrogen, and carbon in the core-shell  $\text{Co}_8\text{FeS}_8@\text{NG}$  hybrid.

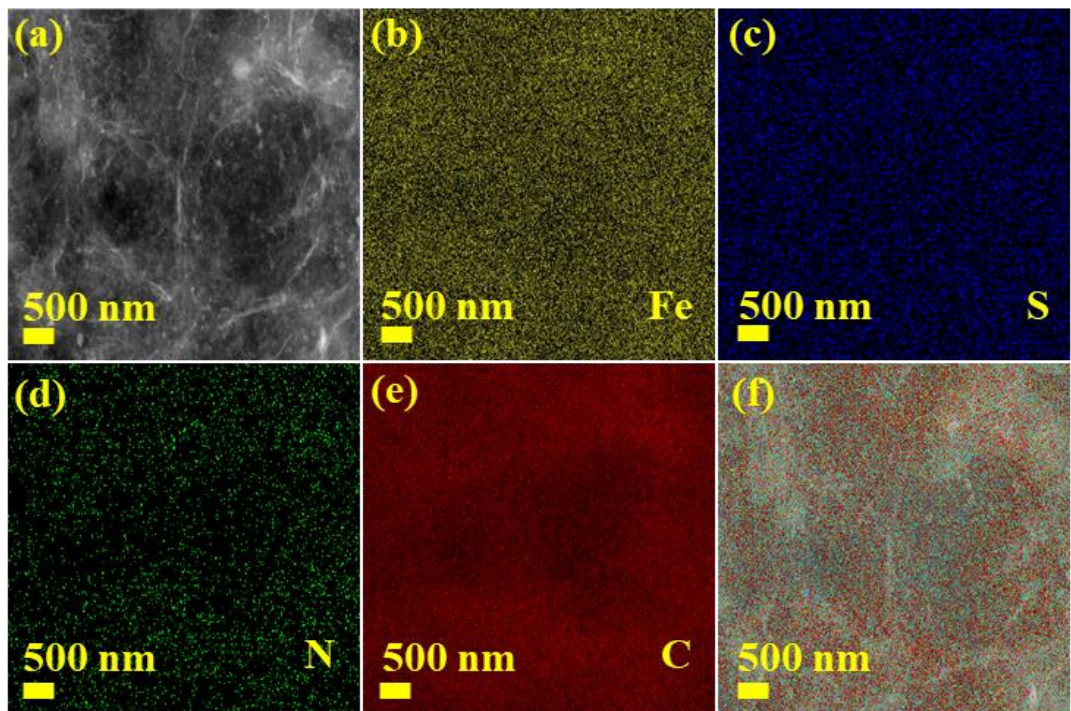


**Fig. S5** SEM-EDS color mapping of iron, sulfur, nitrogen, and carbon, in the  $\text{FeS}@\text{NG}$  hybrid.

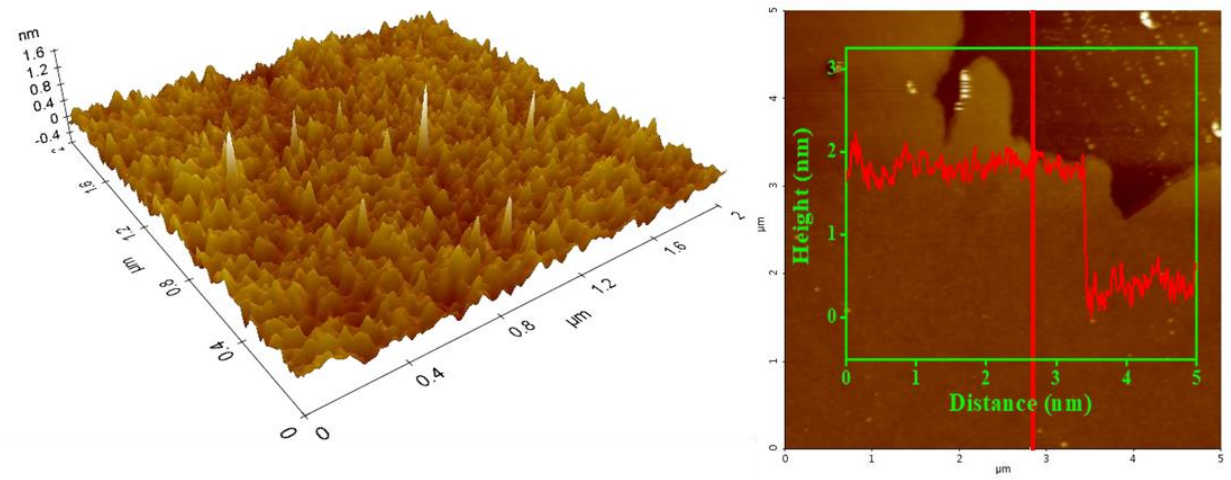


**Fig. S6** AFM images of the core-shell Co<sub>8</sub>FeS<sub>8</sub>@NG hybrid.

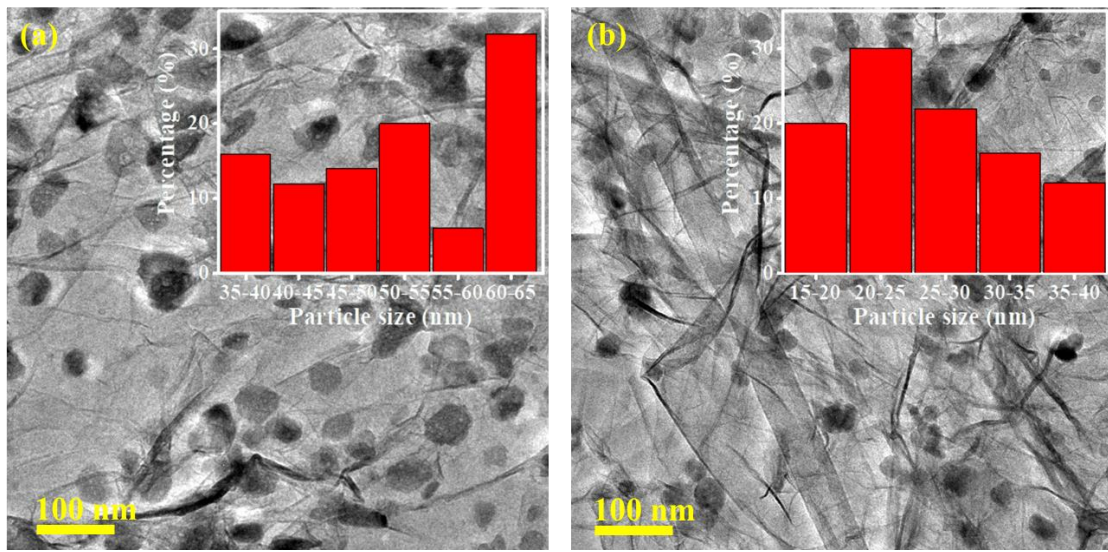


**Fig. S7** (a and b) TEM images of the Co<sub>9</sub>S<sub>8</sub>@NG and FeS@NG hybrids (inset shows their corresponding particle size distributions).

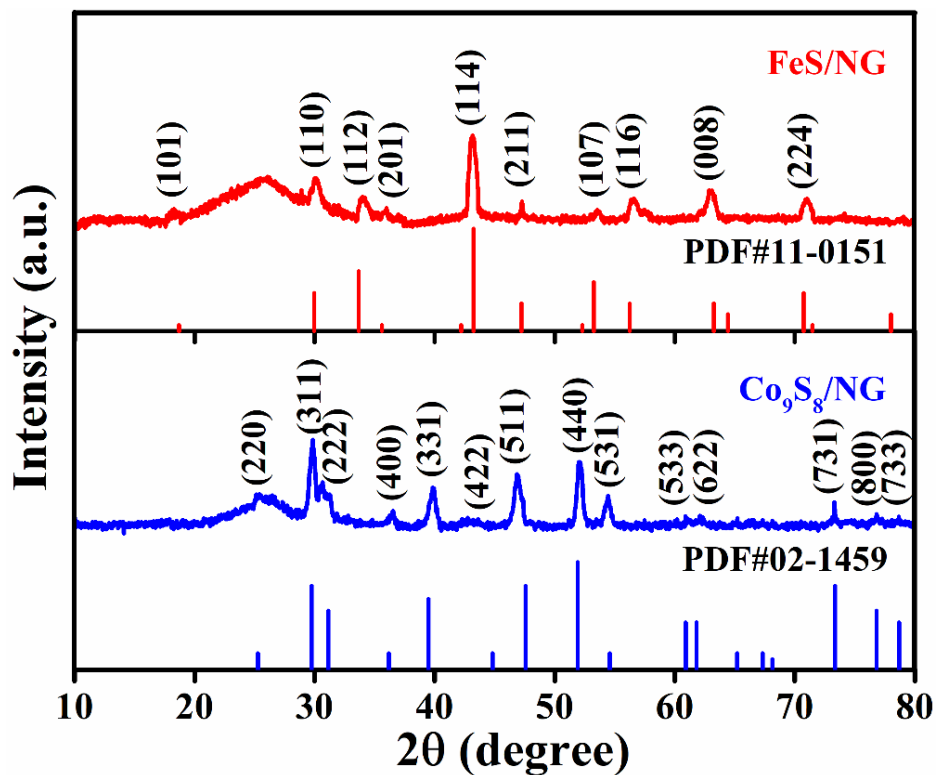


**Fig. S8** XRD pattern of the Co<sub>9</sub>S<sub>8</sub>@NG and FeS@NG hybrids.

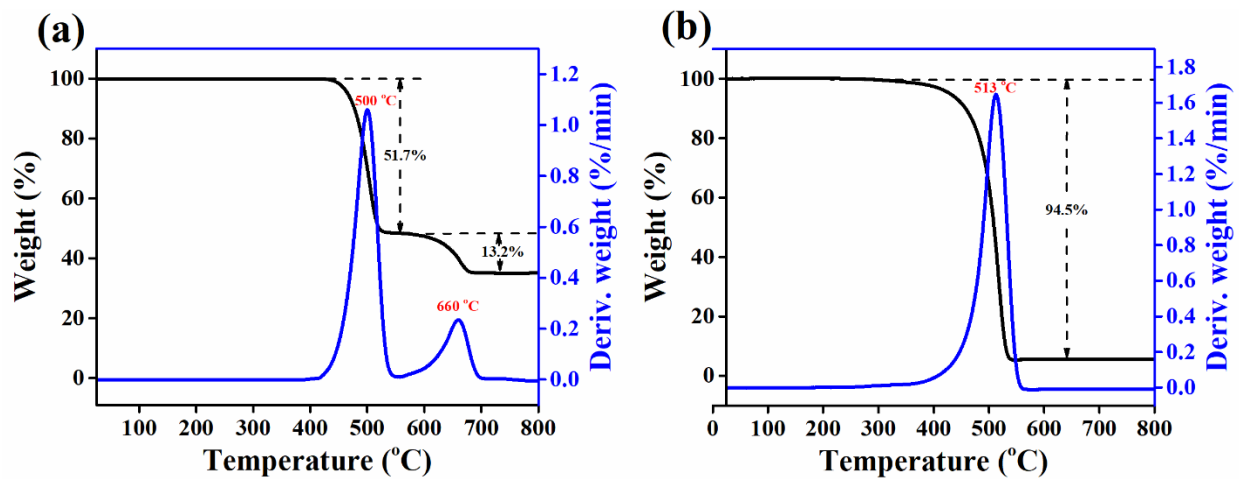


**Fig. S9** TGA-DTA analysis curves of (a) the core-shell  $\text{Co}_8\text{FeS}_8@\text{NG}$  hybrid and (b) Pristine NG.

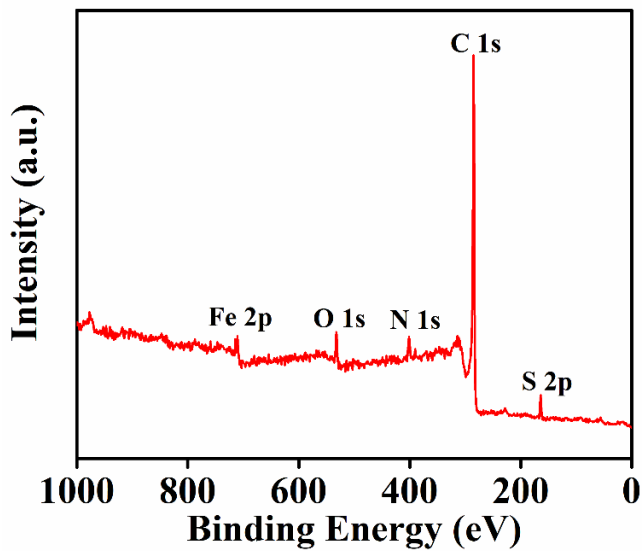


**Fig. S10** XPS survey spectra of the FeS@NG hybrid (negative electrode).

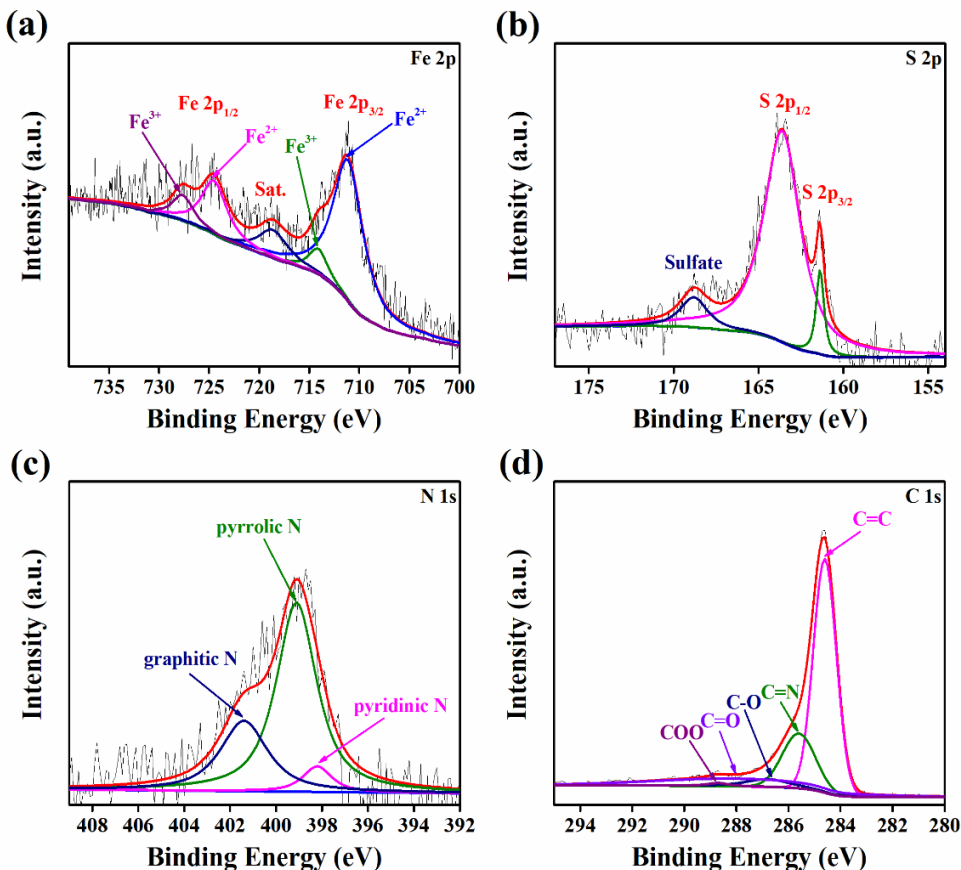


**Fig. S11** High-resolution XPS spectra of a) Fe 2p, b) S 2p, c) N 1s, and c) C 1s, for the FeS@NG hybrid (negative electrode).

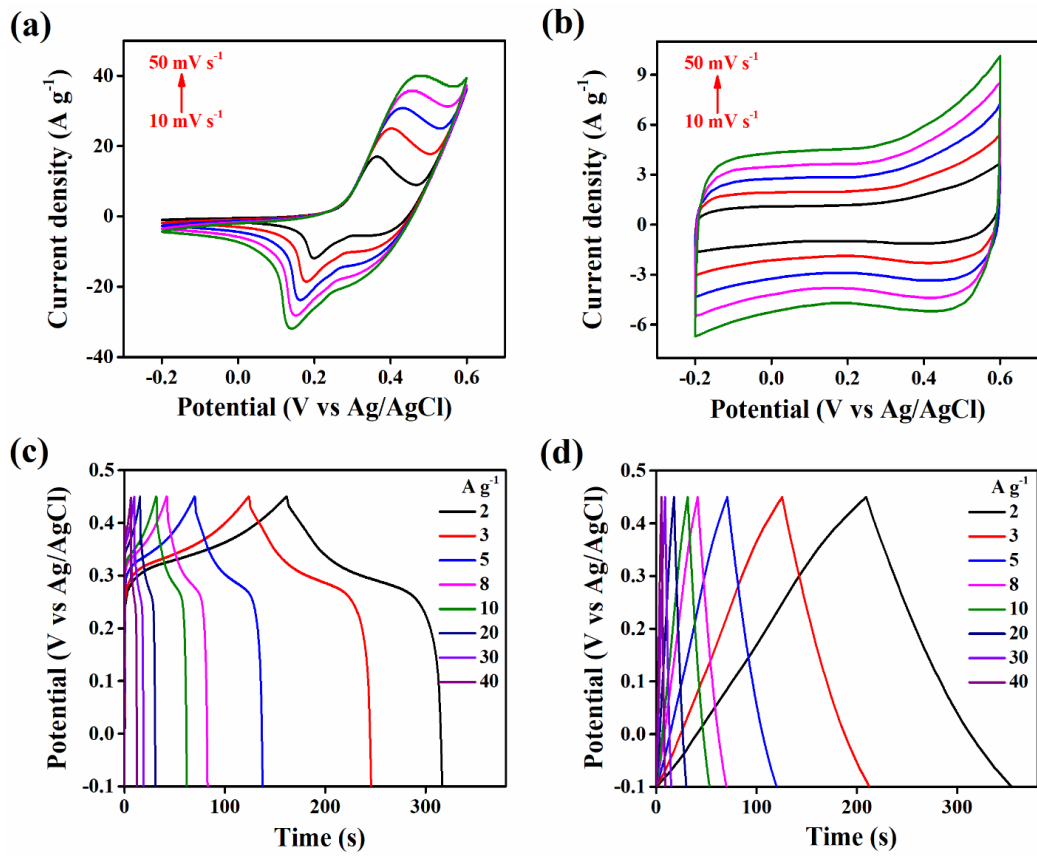


**Fig. S12** CV curves of (a) Pristine Co<sub>8</sub>FeS<sub>8</sub> and (b) Pristine NG electrodes with different scan rates from 10 to 50 mV s<sup>-1</sup>. GCD curves of (c) Pristine Co<sub>8</sub>FeS<sub>8</sub> and (d) Pristine NG electrodes with various current densities from 2 to 40 A g<sup>-1</sup>.

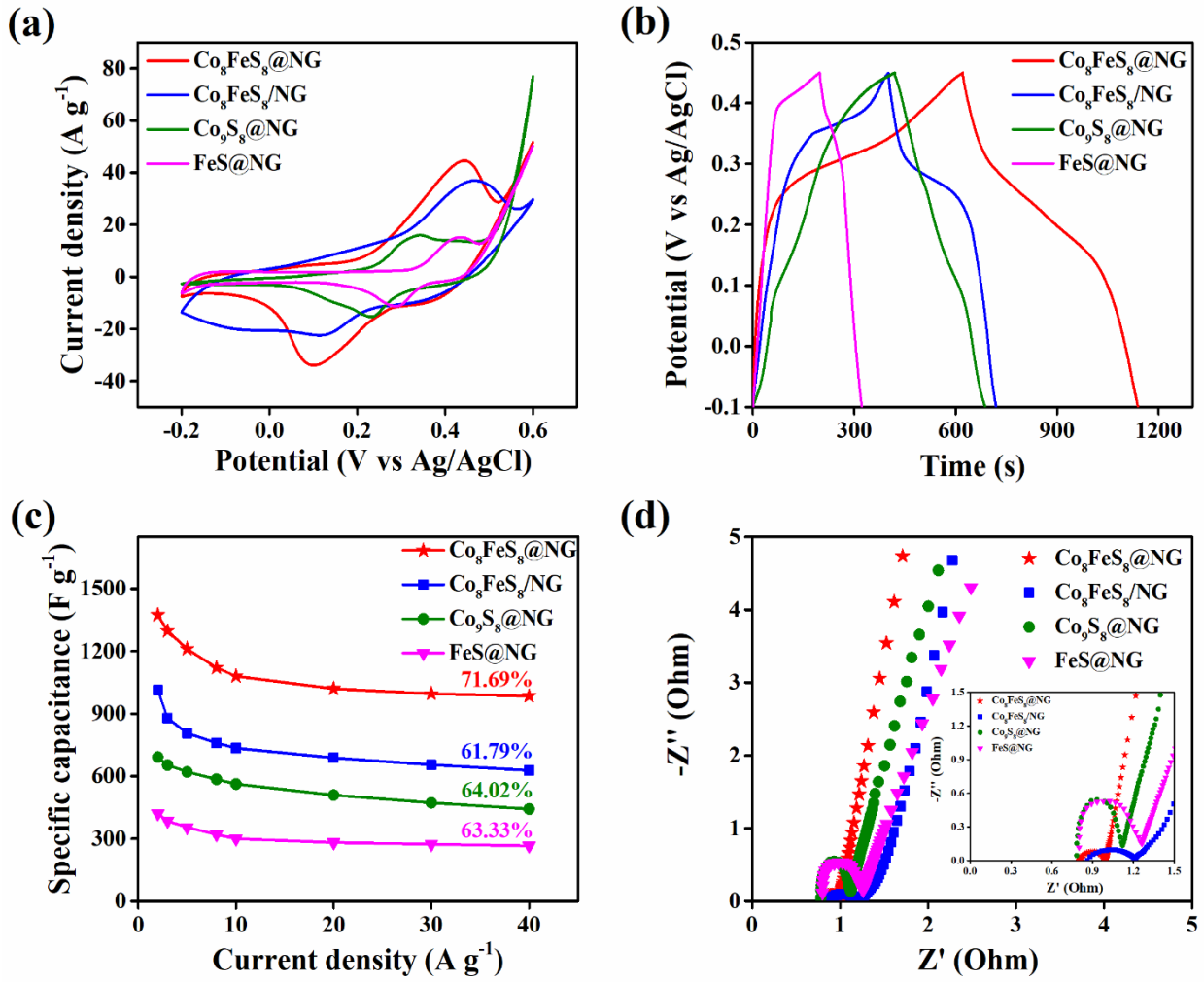


**Fig. S13** (a) CV curves of  $\text{Co}_8\text{FeS}_8@\text{NG}$ ,  $\text{Co}_8\text{FeS}_8/\text{NG}$ ,  $\text{Co}_9\text{S}_8@\text{NG}$ , and  $\text{FeS}@\text{NG}$  electrodes at a scan rate of  $20 \text{ mV s}^{-1}$ , (b) GCD curves of  $\text{Co}_8\text{FeS}_8@\text{NG}$ ,  $\text{Co}_8\text{FeS}_8/\text{NG}$ ,  $\text{Co}_9\text{S}_8@\text{NG}$ , and  $\text{FeS}@\text{NG}$  electrodes at a current density of  $2 \text{ A g}^{-1}$ , (c) Specific capacitance vs. current density of  $\text{Co}_8\text{FeS}_8@\text{NG}$ ,  $\text{Co}_8\text{FeS}_8/\text{NG}$ ,  $\text{Co}_9\text{S}_8@\text{NG}$ , and  $\text{FeS}@\text{NG}$  electrodes, and (d) EIS spectrum of  $\text{Co}_8\text{FeS}_8@\text{NG}$ ,  $\text{Co}_8\text{FeS}_8/\text{NG}$ ,  $\text{Co}_9\text{S}_8@\text{NG}$ , and  $\text{FeS}@\text{NG}$  electrodes.

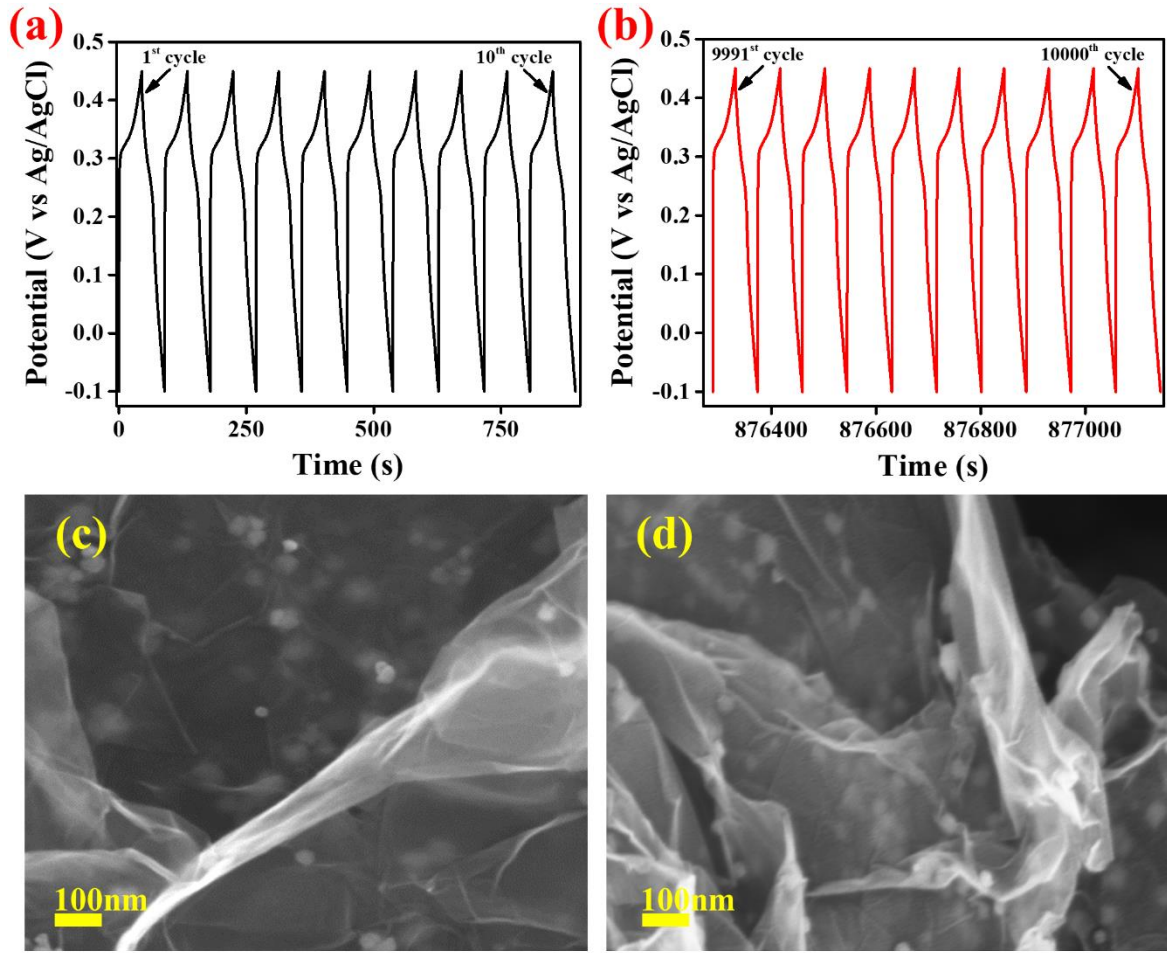


**Fig. S14** GCD curves of  $\text{Co}_8\text{FeS}_8@\text{NG}$  electrode: (a) From 1<sup>st</sup> to 10<sup>th</sup> cycle, (b) From 9991<sup>st</sup> to 10 000<sup>th</sup> cycle, and (c and d) FE-SEM image of core-shell  $\text{Co}_8\text{FeS}_8@\text{NG}$  hybrid before and after 10 000 GCD cycles test, respectively.

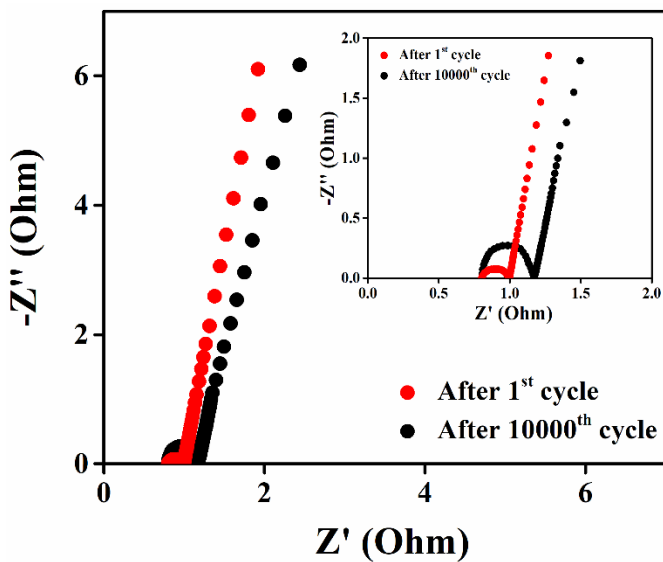


**Fig. S15** EIS spectrum of the Co<sub>8</sub>FeS<sub>8</sub>@NG electrode after 1<sup>st</sup> GCD cycle and after the 10 000<sup>th</sup> GCD cycle.

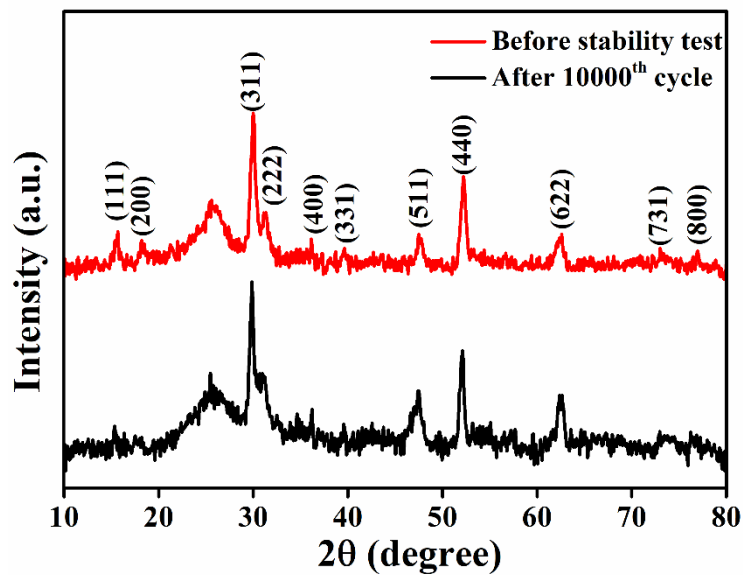


**Fig. S16** XRD pattern of the core-shell Co<sub>8</sub>FeS<sub>8</sub>@NG hybrid before and after cyclic stability test.

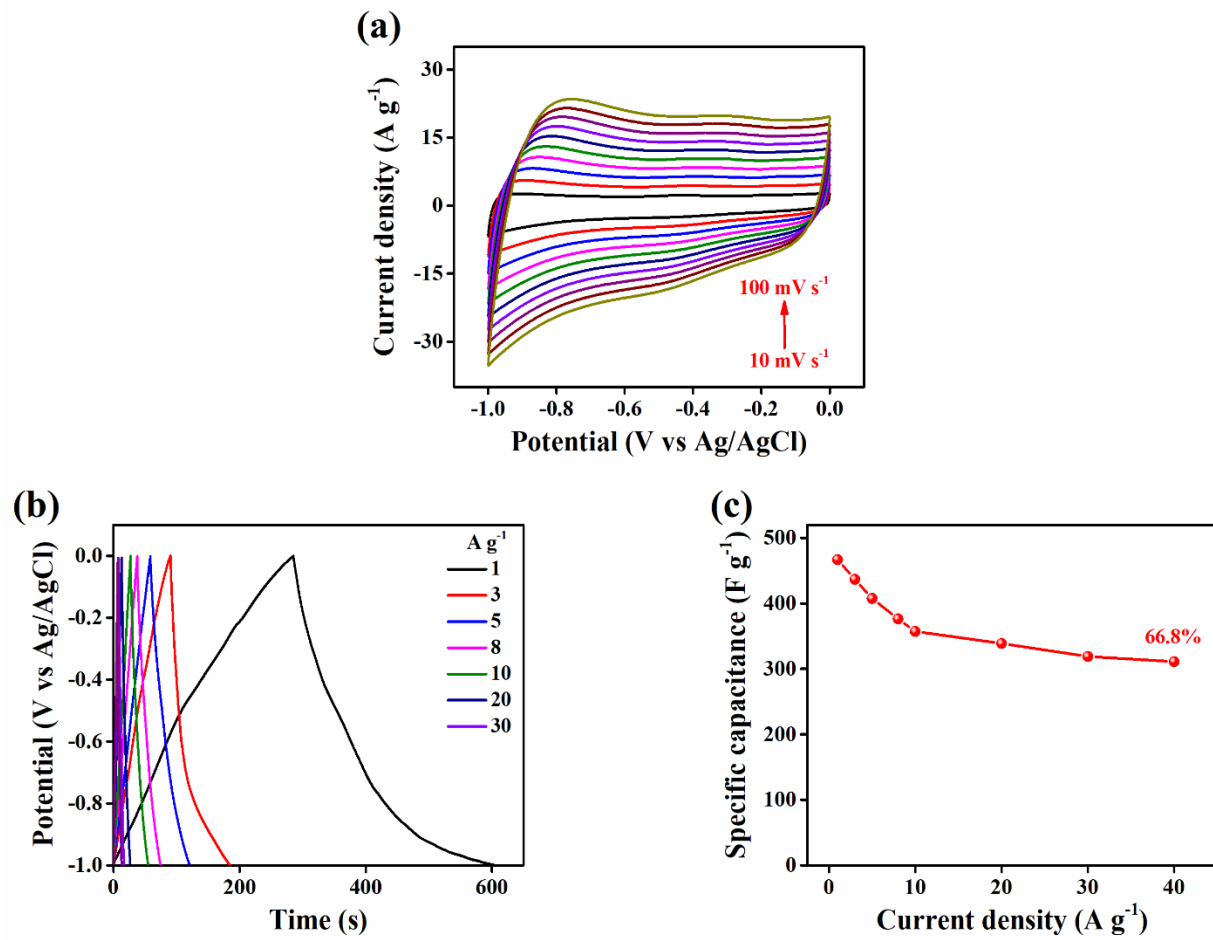


**Fig. S17** (a) CV curves of the FeS@NG electrode at different scan rates from 10 to 100 mV s<sup>-1</sup>, (b) GCD curves of FeS@NG electrode at various current densities from 1 to 30 A g<sup>-1</sup>, and (c) Specific capacitance *vs.* current density of FeS@NG electrode.

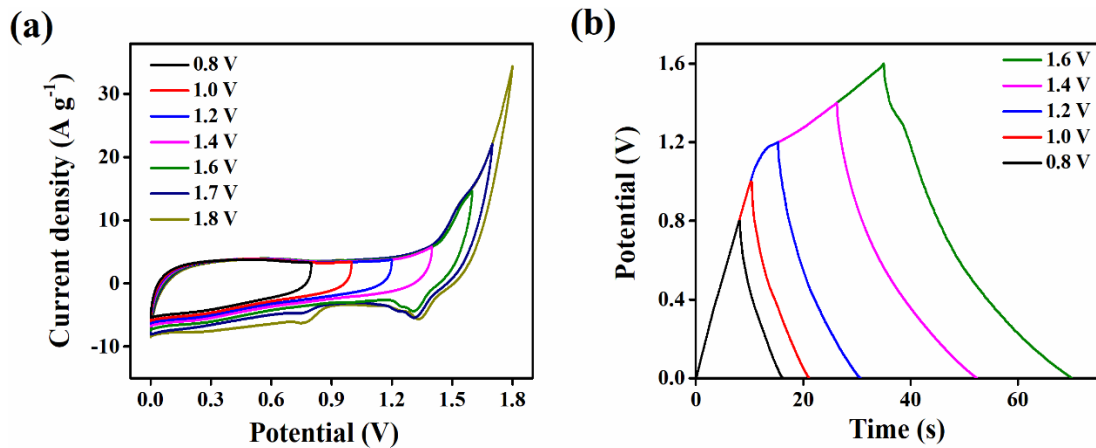


**Fig. S18** (a) CV curves (at a sweep rate of  $20 \text{ mV s}^{-1}$ ) of the  $\text{Co}_8\text{FeS}_8@\text{NG}/\text{FeS}@\text{NG}$  ASC device with different operating potential window from 0.8 to 1.8 V and (b) GCD curves (at a current density of  $10 \text{ A g}^{-1}$ ) of the  $\text{Co}_8\text{FeS}_8@\text{NG}/\text{FeS}@\text{NG}$  ASC device at different operating potential window from 0.8 to 1.6 V.

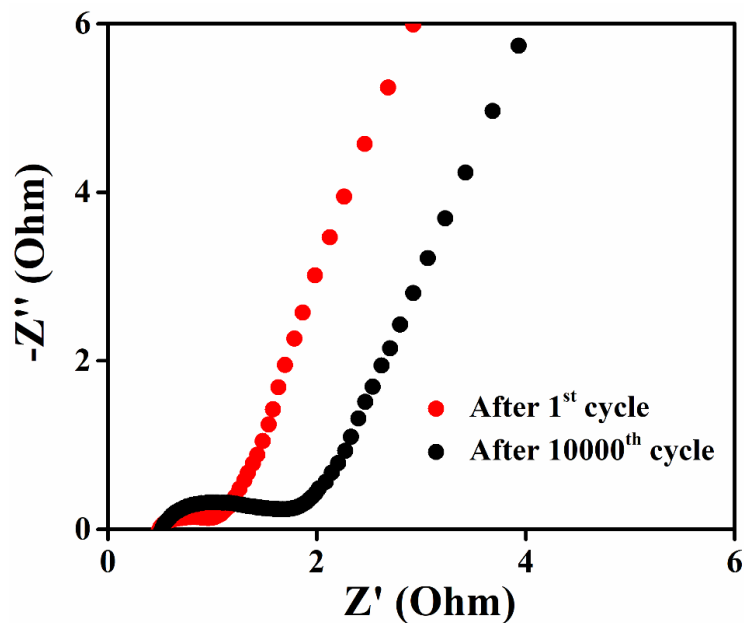


**Fig. S19** EIS spectrum of the  $\text{Co}_8\text{FeS}_8@\text{NG}/\text{FeS}@\text{NG}$  ASC after the 1<sup>st</sup> and 10 000<sup>th</sup> cycles test.

**Table S1.** Elemental composition of the core-shell Co<sub>8</sub>FeS<sub>8</sub>@NG and FeS@NG hybrids measured by XPS analysis.

Sample	Co (at. %)	Fe (at. %)	S (at. %)	N (at. %)	C (at. %)	O (at. %)
Co <sub>8</sub> FeS <sub>8</sub> @NG	4.11	1.12	5.49	6.26	76.10	6.92
FeS@NG	-	3.88	3.41	6.12	79.2	7.39

**Table S2.** Electrochemical properties of the Co<sub>8</sub>FeS<sub>8</sub>@NG electrode comparison with reported literature.

Materials	Specific capacitance (F g <sup>-1</sup> )	Current density	Electrolyte	Potential window (V)	Stability (Cycles)	References
Co <sub>8</sub> FeS <sub>8</sub> @NG	1374	2 A g <sup>-1</sup>	2 M KOH	-0.1-0.45	96.1% (10 000)	This work
GNS/NiS	775	0.5 A g <sup>-1</sup>	6 M KOH	0.0-0.4	88.1% (1000)	1
NiCo <sub>2</sub> S <sub>4</sub> -g-MoS <sub>2</sub>	1002	5 A g <sup>-1</sup>	6 M KOH	0-0.3	94.8% (4000)	2
GN-CoMoS <sub>4</sub> @rGO	774	1 A g <sup>-1</sup>	3 M KOH	0.0-0.55	94.49% (6000)	3
Ni <sub>x</sub> Co <sub>1-x</sub> S <sub>1.987</sub> microspheres/rGO	1152	0.5 A g <sup>-1</sup>	2 M KOH	0.0-0.5	-	4
CGH	564	1 A g <sup>-1</sup>	6 M KOH	-0.05-0.4	94.8% (2000)	5
CoMoS <sub>4</sub>	661	1 A g <sup>-1</sup>	1 M KOH	0.0-0.6	86% (10 000)	6
ZnCo <sub>1-x</sub> S nanoartichokes	486	2 A g <sup>-1</sup>	1 M KOH	0.0-0.45	86.4% (2000)	7
CdS/NF	909	2 mA cm <sup>-2</sup>	6 M KOH	0.0-0.4	104% (5000)	8
Co <sub>2</sub> CuS <sub>4</sub> /NG	1005	1 A g <sup>-1</sup>	6 M KOH	-0.1-0.5	96.3% (5000)	9
Ni <sub>3</sub> S <sub>2</sub> @Ni(OH) <sub>2</sub> /3D GN	1277	5.1 A g <sup>-1</sup>	3 M KOH	-0.15-0.55	99.1% (2000)	10

CGH: 3D CoS/graphene composite hydrogel

**Table S3.** ASCs device performance comparison with previously reported literature.

<b>Reported ASC Devices</b>	<b>Electrolyte</b>	<b>Device window (V)</b>	<b>Energy density (Wh kg<sup>-1</sup>)</b>	<b>Power density (kW kg<sup>-1</sup>)</b>	<b>Stability (Cycles)</b>	<b>References</b>
Co <sub>8</sub> FeS <sub>8</sub> @NG//FeS@NG	PVA-KOH	0-1.6	70.4	0.59	93.7% (10 000)	This work
Ni-Co-S/G//PCNS	KOH	0-1.6	43.3	0.8	85% (10000)	11
ZICO//NG	PVA-KOH	0-1.5	40.5	0.75	95% (5000)	12
GN-CoMoS <sub>4</sub> @rGO//AC	PVA-KOH	0-1.8	42.8	0.9	93.2% (8000)	3
CuCo <sub>2</sub> S <sub>4</sub> @NiMn-LDH//AC	KOH	0-1.5	45.8	1.49	87.6% (10 000)	13
Fe <sub>3</sub> O <sub>4</sub> @Fe <sub>2</sub> O <sub>3</sub> /Fe <sub>3</sub> O <sub>4</sub> @MnO <sub>2</sub>	Na <sub>2</sub> SO <sub>4</sub>	0-2.0	26.6	0.5	92% (5000)	14
CC@CoMoO <sub>4</sub> @NiCo-LDH	PVA-KOH	0-1.6	59.5	0.8	89.7% (5000)	15
MnO <sub>2</sub> NS-CC//FeOOH NS-CC	Li <sub>2</sub> SO <sub>4</sub>	0-1.85	37.4	16	-	16
MoO <sub>2</sub> @NC//CuCo <sub>2</sub> S <sub>4</sub>	PVA-KOH	0-1.6	65.1	0.8	90.6% (5000)	17
Co <sub>2</sub> CuS <sub>4</sub> /NG//NG	KOH	0-1.6	53.3	0.79	92.2% (4000)	9
NiNTAs@MnO <sub>2</sub> //NiNTAs@Fe <sub>2</sub> O <sub>3</sub>	PVA-Na <sub>2</sub> SO <sub>4</sub>	0-1.6	34.1	3.19	79.3% (5000)	18
NiCo <sub>2</sub> S <sub>4</sub> //AC	KOH	0-1.5	28.3	0.24	91.7% (5000)	19

## Notes and References

- 1 Y. Li, K. Ye, K. Cheng, J. Yin, D. Cao and G. Wang, *J. Power Sources*, 2015, **274**, 943–950.
- 2 J. Shen, P. Dong, R. Baines, X. Xu, Z. Zhang, P. M. Ajayan and M. Ye, *Chem. Commun.*, 2016, **52**, 9251–9254.
- 3 M. Wei, C. Wang, Y. Yao, S. Yu, W. H. Liao, J. Ren, R. Sun and C. P. Wong, *Chem. Eng. J.*, 2019, **355**, 891–900.
- 4 Y. Gao, L. Mi, W. Wei, S. Cui, Z. Zheng, H. Hou and W. Chen, *ACS Appl. Mater. Interfaces*, 2015, **7**, 4311–4319.
- 5 X. Meng, J. Deng, J. Zhu, H. Bi, E. Kan and X. Wang, *Sci. Rep.*, 2016, **6**, 1–9.
- 6 X. Xu, Y. Song, R. Xue, J. Zhou, J. Gao and F. Xing, *Chem. Eng. J.*, 2016, **301**, 266–275.
- 7 J. Yang, Y. Zhang, C. Sun, G. Guo, W. Sun, W. Huang, Q. Yan and X. Dong, *J. Mater. Chem. A*, 2015, **3**, 11462–11470.
- 8 P. Xu, J. Liu, P. Yan, C. Miao, K. Ye, K. Cheng, J. Yin, D. Cao, K. Li and G. Wang, *J. Mater. Chem. A*, 2016, **4**, 4920–4928.
- 9 M. Guo, J. Balamurugan, T. D. Thanh, N. H. Kim and J. H. Lee, *J. Mater. Chem. A*, 2016, **4**, 17560–17571.
- 10 W. Zhou, X. Cao, Z. Zeng, W. Shi, Y. Zhu, Q. Yan, H. Liu, J. Wang and H. Zhang, *Energy Environ. Sci.*, 2013, **6**, 2216–2221.
- 11 J. Yang, C. Yu, X. Fan, S. Liang, S. Li, H. Huang, Z. Ling, C. Hao and J. Qiu, *Energy Environ. Sci.*, 2016, **9**, 1299–1307.
- 12 A. Maitra, A. K. Das, R. Bera, S. K. Karan, S. Paria, S. K. Si and B. B. Khatua, *ACS Appl. Mater. Interfaces*, 2017, **9**, 5947–5958.
- 13 J. Lin, H. Jia, H. Liang, S. Chen, Y. Cai, J. Qi, C. Qu, J. Cao, W. Fei and J. Feng, *Chem. Eng. J.*, 2018, **336**, 562–569.
- 14 X. Tang, R. Jia, T. Zhai and H. Xia, *ACS Appl. Mater. Interfaces*, 2015, **7**, 27518–27525.

- 15 Y. Zhao, X. He, R. Chen, Q. Liu, J. Liu, J. Yu, J. Li, H. Zhang, H. Dong, M. Zhang and J. Wang, *Chem. Eng. J.*, 2018, **352**, 29–38.
- 16 Y.-C. Chen, Y.-G. Lin, Y.-K. Hsu, S.-C. Yen, K.-H. Chen and L.-C. Chen, *Small*, 2014, **10**, 3803–3810.
- 17 S. Liu, Y. Yin, K. S. Hui, K. N. Hui, S. C. Lee and S. C. Jun, *Adv. Sci.*, 2018, **5**, 1800733.
- 18 Y. Li, J. Xu, T. Feng, Q. Yao, J. Xie and H. Xia, *Adv. Funct. Mater.*, 2017, **27**, 26–28.
- 19 Y. Zhu, Z. Wu, M. Jing, X. Yang, W. Song and X. Ji, *J. Power Sources*, 2015, **273**, 584–590.